Applied Catalysis B: Environmental 189 (2016) 242–251

Contents lists available at ScienceDirect

Applied Catalysis B: Environmental

journal homepage: www.elsevier.com/locate/apcatb

Pd nanoparticles encapsulated into mesoporous ionic copolymer: Efficient and recyclable catalyst for the oxidation of benzyl alcohol with O_2 balloon in water

Qian Wang, Xiaochun Cai, Yangqing Liu, Jingyan Xie, Yu Zhou*, Jun Wang*

State Key Laboratory of Materials-Oriented Chemical Engineering, College of Chemical Engineering, Nanjing Tech University, Nanjing 210009, China

ARTICLE INFO

Article history:
Received 3 December 2015
Received in revised form 1 February 2016
Accepted 28 February 2016
Available online 2 March 2016

Keywords:
Palladium
Poly(ionic liquid)s
Nanocatalysis
Porous materials
Selective oxidation

ABSTRACT

A series of functional cross-linked mesoporous poly(ionic liquid)s (MPILs) were prepared through the free radical copolymerization of divinylbenzene (DVB) and imidazolium salts based ionic liquids tethered with different groups (−COOH, C_4H_9, −CN and $-NH_2$). These MPILs were applied as supports to prepare immobilized palladium (Pd) nanoparticles (NPs) through ion exchanging with sodium tetrachloropalladate(II) (Na_2PdCl_4) and successive reduction by sodium borohydride ($NaBH_4$). Highly uniform and narrow dispersed Pd NPs attained on the carboxyl modified MPIL with large surface area and high ionic density. The obtained materials acted as an efficient and stable recycling heterogeneous catalyst for the atmospheric pressure oxidation of benzyl alcohol to benzaldehyde by using O_2 as the oxidant and water as the sole solvent at low temperature (90 °C). The special ionic framework with −COOH group plays a major role in the formation and stabilization of ultrafine Pd NPs. This work indicates that controlling the textural properties of ionic copolymers serves as a facile and efficient way to fabricate immobilized stable metal NPs.

1. Introduction

Noble metallic nanoparticles (NPs) have attracted continuous and growing attentions in chemistry and material sciences due to the quantum size effect, high ratio of surface area to volume, and so on [1,2]. Especially, they serve as highly efficient catalysts for many organic reactions, among which, palladium (Pd) NPs has been extensively studied [3–6]. Owing to the high price of noble metals, easy separation and stable reuse of the noble metal catalysts are mostly desirable, in addition to exploration of their high catalytic efficiency. For this purpose, many noble metallic NPs are immobilized onto suitable supports so as to heterogenize noble metal catalysts [7]. For decades, it is a hotspot of research to improve the catalytic efficiency of supported noble metallic NPs, which depends on the control of particle size, dispersion, distribution and stabilization on the selected support toward the requirement of target reactions [8].

A great number of supports have been developed for immobilization of noble metallic NPs, including numerous inorganic porous materials, inorganic-organic hybrids and organic polymers [9–14]. Porous organic polymes (POPs) having large surface areas and tunable pore structures enable high dispersion of guest NPs. Also, the surface state can be facilely functionalized to afford sufficient affinity to metal precursors, through which the loaded NPs can be stabilized by coordination interaction, hydrogen bonds, etc [15–17]. Moreover, the versatile surface states and organic frameworks benefit accessibility of organic substrates, thus POPs-supported noble metallic NPs are particularly suitable for catalyzing low-temperature liquid-solid heterogeneous organic reactions [18]. In contrast to the neutral framework of organic POPs, zeolites are traditional microporous inorganic materials with anionic skeleton; through cation-exchange, metal ions can be facilely introduced into zeolitic frameworks [19,20]. If the cation-exchange is followed by a chemical reduction treatment, finely dispersed metal clusters can be achieved within zeolite micropores [21]. It is notable that poly(ionic liquid) s (PILs) are a new member of ionic polymer materials [22,23], and a number of mesoporous poly(ionic liquid) s (MPILs) have been successful prepared and applied as novel heterogeneous catalysts or catalyst supports [24].

* Corresponding authors.
E-mail addresses: njutzhouyu@njtech.edu.cn (Y. Zhou), junwang@njtech.edu.cn (J. Wang).

http://dx.doi.org/10.1016/j.apcatb.2016.02.067
0926-3373/

Very recently, MPILs with polymerized organic cation backbones are emerging quickly, which could be prepared from free radical copolymerization [25], free radical self-polymerization [26,27], and nucleophilic substitution reactions [28,29]. One common feature of these cation-backbone MPILs is that they can be functionalized with anion-exchange. Thus, when used as supports for noble metallic NPs, MPILs not only can show the features of porous polymers like POPs, but also would exhibit several additional advantages. (1) They enable the loading of NPs through anion-exchange with successive chemical reduction, just like the cation-exchange immobilization mode on zeolites. (2) Electrostatic interaction provided by ionic sites can stabilize the incorporated NPs, similar to the stabilization effect of NPs in ionic liquids (ILs) [30,31]. (3) The task-specifically designed IL monomer is not only for polymerization but possibly as a catalytic promoter in backbone. Despite above advantages, rare report is related to the NPs encapsulated into MPILs via anion-exchange and chemical reduction [29]. Further for ionic copolymer, meso- and macropores can be conveniently constructed from free radical copolymerization of IL monomer and divinylbenzene (DVB) without using any templates, in which tethering the IL monomer with a functional ligand is feasible, potentially very useful to assisting stabilization of NPs. Also, constructed meso- and macro pores facilitate the supporting of NPs and improve the mass transfer in heterogeneous catalysis. More importantly, adjustment of hydrophilic/hydrophobic property is achieved by altering the ratio of hydrophilic IL unit and hydrophobic DVB. This strategy allows fabricating amphipathic organic pore walls that favor accessibility of both organic substrate and water, thus benefit the use of water as green solvent for some liquid-liquid biphasic organic syntheses. However, up to date, none mesoporous ionic copolymer has been applied as the support of noble metallic NPs, including Pd NPs.

Pd NPs are well-known as the effective catalysts for numerous selective hydrogenation and oxidation reactions [32,33]. In latter area, selective oxidation of alcohols is the most important process for producing aldehydes and ketones in organic syntheses, wherein benzyl alcohol is one of the most representative substrates and its oxidation has been broadly studied as a model reaction, as well as for practical application [34]. A wide variety of supports were used to immobilize Pd NPs for the oxidation of benzyl alcohol to benzaldehyde with O_2 [35–37]. For purpose of environmental-benign and energy-saving, solvent-free catalysis at a high temperature or using water as green solvent at a low temperature is nowadays pursuit for this reaction [38]. However, the efficiency and/or stability of the currently available supported Pd NPs are still unsatisfactory, and it is still one challenge to develop the highly efficient and steadily recyclable Pd NPs for aerobic oxidation of benzyl alcohol in water under mild conditions.

In this work, we initiate the application of mesoporous ionic copolymers for fabrication of the supported Pd NPs, and study their catalytic performance in oxidation of benzyl alcohol with O_2 as oxidant and water as solvent. This kind of MPILs is synthesized through the free radical copolymerization of divinylbenzene (DVB) and imidazolium-based ILs respectively tethered with −COOH, $-C_4H_9$, −CN and $-NH_2$. The MPIL-supported Pd NPs is prepared via the two-step approach of anion-exchange and successive reduction by sodium borohydride ($NaBH_4$). Our step-by-step analysis on structure-performance relationship reveals that the highly dispersed and sufficiently stabilized Pd NPs are attained on the surface of carboxyl functional MPIL with large surface area and high ionic density simultaneously. It exhibits superior activity and excellent recyclability in the oxidation of benzyl alcohol to benzaldehyde by using O_2 as the oxidant and water as the sole solvent at atmospheric pressure and low temperature of 90 °C. Nano size, narrow distribution and well stabilized Pd particles, as well as the amphipathic organic mesopore surface, account for the excellent performance.

2. Experimental

2.1. Materials and method

All reagents were commercially available and used as received without further purification. The chemicals were all of analytical grade. ^{1}H NMR spectra and ^{13}C NMR spectra were acquired on a Bruker DPX 500 spectrometer at ambient temperature by using D_2O as solvent and TMS (tetramethylsilane) as internal reference. Fourier transform infrared spectroscopy (FTIR) spectra were recorded on an Agilent Cary 660 FT-IR instrument (KBr disks) ranging from 4000 to 400 cm^{-1}. Elemental analyses were performed with a CHN elemental analyzer Vario EL cube. The nitrogen sorption isotherms and pore size distribution curves were measured at the temperature of liquid nitrogen (77 K) by using a BELSORP-MINI analyser with the samples being degassed at 80 °C for 3 h before analysis. XRD patterns were collected on a Smart Lab diffractmeter from Rigaku equipped with a 9 kW rotating anode Cu source at 45 kV and 200 mA from 5° to 80° with a scan rate of 0.2° s^{-1}. Scanning electron microscopic (SEM) images were viewed on a Hitachi S-4800 field-emission scanning electron microscope. Transmission electron microscopy (TEM) analysis was performed on a JEM-2100 (JEOL) electron microscope operating at 200 kV. The X-ray photoelectron spectra (XPS) was conducted on a PHI 5000 Versa Probe X-ray photoelectron spectrometer equipped with Al Karadiation (1486.6 eV). Thermogravimetric (TG) analysis was performed with an STA409 instrument in dry air atmosphere at a heating rate of 10 °C min^{-1}. Solid state ^{13}C NMR spectra were originally recorded in a Bruker AVANCE-III spectrometer in a magnetic field strength of 9.4 T corresponding to the Larimore frequency of 100 MHz for ^{13}C nuclei with a CP/MAS unit at room temperature. The spinning rate and contact time were 12 kHz and 2.5 ms, respectively. The pulse width, spectral width, and acquisition time was 3.0 μs, 300.0 kHz, and 33.91 ms; for each spectrum, 10000 scans were accumulated. The reaction liquid was analyzed by a gas chromatography (Agilent 7890B) equipped with a FID detector and a capillary column (HP-5, 30m × 0.25mm × 0.25 μm).

2.2. Catalyst preparation

2.2.1. Preparation of IL monomer VPA-HBr

3-bromopropionic acid (3.06 g, 0.02 mol) was dissolved in anhydrous ethanol (20 mL), and 1-vinylimidazole (1.811 g, 0.2 mol) was added drop slowly to the solution. The mixture was refluxed for 24 h at 75 °C. After cooled to room temperature, the reaction mixture was spin steamed to obtain the thick liquid. A white solid precipitated by adding anhydrous acetonitrile (20 mL) and then was separated by filtration, washed with acetonitrile for several times, and vacuum dried at 50 °C for 24 h to give the final light white solid, the IL monomer ([1-vinyl-3-propane carboxylation imidazolium]Br) VPA-HBr (4.5 g, 90% yield). Found: N, 11.24%; C, 38.93%; H, 4.078%; on theory: N, 11.24%; C, 38.86%; H, 4.42%. ^{1}H NMR (300 MHz, D_2O, TMS) for VPA-HBr δ (ppm) = 3.01 (t, 2H, $-CH_2$), 4.72 (t, 2H,-CH_2), 5.45 (m, 1H, −CH), 5.81 (m, 1H, −CH), 7.17 (m, 1H, −CH), 7.63 (s, 1H, −CH), 7.79 (s, 1H, −CH), 9.12 (s, 1H, −CH) (see Fig. S1). The ^{1}H NMR of other functional liquids lies on support (see Fig. S2–S4)

2.2.2. Preparation of ionic copolymer

Ionic copolymers were prepared through free radical copolymerization of IL monomer VPA-HBr and divinylbenzene (DVB) by using azobisisobutyronitrile (AIBN) as initiator [39]. In as typical synthesis, VPA-HBr (1.235 g, 5 mmol), DVB (0.716 g, 5.5 mmol) and

Table 1
Textural properties of MPILs.

Entry	Catalyst support	IL:DVB (mol/mol)	IL Cont. (mmol g^{-1})[a]	S_{BET} (m^2 g^{-1})[b]	V_p (cm^3 g^{-1})[c]	D_p (nm)[d]
1	PDC(0.10)	0.10:1	0.75	10	0.062	–
2	PDC(0.17)	0.17:1	0.75	39	0.072	3.72
3	PDC(0.35)	0.35:1	0.98	84	0.201	3.72
4	PDC(0.70)	0.7:1	1.71	310	0.203	2.61
5	PDC(1.00)	1:1	2.27	174	0.150	3.72
6	PDVB	0:1	0	259	0.195	3.00
7	PIL-NH_2	1:1	0.50	101	0.441	2.43
8	PIL-C_4H_9	1:1	2.16	93	0.106	3.72
9	PIL-CN	1:1	0.96	103	0.269	3.29

[a] IL content in MPILs calculated from elemental analysis.
[b] BET surface area.
[c] Total pore volume.
[d] Average pore size.

AIBN (0.09 g, 0.55 mmol) were dissolved in a mixture solution containing anhydrous ethanol (5 mL), water (5 mL) and ethyl acetate (25 mL), and then refluxed with string at 80 °C for 24 h. A white solid formed in the flask, and was collected by filtration, washed with water for three times, and dried at 50 °C in the vacuum drying oven for 12 h. Dry solid of 1.2 g was obtained with 62% yield. By varying the initial molar ratio of VPA-HBr and DVB, a series ionic copolymers tethered with −COOH group were prepared and named as PDC(n) (n = 0.10, 0.17, 0.35, 0.70 and 1, Table 1), in which n denoted the initial molar ratio of IL to DVB.

For comparison, various other ionic copolymers tethered with different groups of $-C_4H_9$, $-NH_2$ and −CN were synthesized with above similar precursor except that replacing VPA-HBr with other corresponding functional IL monomers. The obtained ionic copolymers were denoted as PIL-C_4H_9, $-NH_2$ and −CN. Homopolymer PDVB was prepared similarly. Details of these syntheses were seen in the Supporting Information.

2.2.3. Preparation of Pd@MPIL

Palladium nanoparticles (Pd NPs) supported on MPIL (Pd@MPIL) was prepared through $NaBH_4$ reduction route. Typically, PIL (0.25 g) was mixed with 20 mL aqueous Na_2PdCl_4 (0.0138 g, 0.047 mmol) solution, and then stirred at room temperature for 12 h. After that, the solid was separated by filtration, washed with deionized water. The above ion-exchanging process was repeated twice and the obtained solid was emerged in 20 mL water containing 0.054 g polyvinyl pyrrolidone (PVP) and 0.52 g sodium dodecyl sulfate (SDS). Successively, 1 mL aqueous sodium borohydride (0.01 g $NaBH_4$) solution was added drop by drop at 5 °C and then treated by ultrasonic wave for 20 min. The solid was separated by filtration, washed with water and then vacuum dried for 12 h to give 0.22 g black solid. Similarly, various other Pd@MPIL materials were prepared by varying the MPIL supports and Pd precursors such as $Pd(OAc)_2$ and $PdCl_2$.

2.3. Oxidation of benzyl alcohol to benzaldehyde

The catalytic performance was assessed by the oxidation of benzyl alcohol with oxygen balloon in green reaction media water. In a typical run, benzyl alcohol (1 mmol), water (1 mL), K_2CO_3 (1 mmol) and catalyst (0.02 g) were successively added in a reaction tube and stirred at 90 °C for five hours with fierce stirring. For accurate analysis of the product, after reaction, ethanol (10 mL) was added to dilute the reaction system. The liquid phase was collected and analyzed by gas chromatography (GC, Agilent 7890B) using toluene as the internal standard for calculation. Conversion (based on benzyl alcohol) = mmol (benzyl alcohol) converted/mmol (initial benzyl alcohol) × 100%, selectivity of benzaldehyde = mmol (benzaldehyde)/mmol (benzyl alcohol converted) × 100%. In order to test the catalytic recyclability, solid catalyst was separated by filtration, washed with ethanol for three times, dried in vacuum at 80 °C for 6 h, and then used for the next run.

3. Results and discussion

3.1. Fabrication and characterization of Pd@MPIL

Scheme 1 shows the preparation procedure of Palladium (Pd) nanoparticles (NPs) supported on mesoporous poly(ionic liquid) (MPIL). The MPIL supports are ionic copolymers synthesized through the free radical copolymerization of IL monomer and DVB by using AIBN as the initiator. Pd NPs are encapsulated into the MPIL matrix through an ion-exchanging process and successive reduction with $NaBH_4$. In above route, a series of carboxyl functional MPIL supports are prepared by using IL monomer (VPA-HBr) tethered with −COOH group. They are named as PDC(n) (n = 0.10, 0.17, 0.35, 0.70 and 1, Table 1), in which n stands for the initial molar ratio of IL to DVB. Correspondingly, Pd loaded samples are named as Pd@PDC(n).

Fig. 1 shows the nitrogen sorption results of these PDC(n) samples. All of them show type IV isotherms (Fig. 1A), index of classical mesopores [40]. The pore-size distribution curves (Fig. 1B) further reveal the existence of mesopores with narrow pore size distribution centered around 3–4 nm. As the IL proportion (n) increases, apparently enhanced nitrogen uptake is observed at the low relative pressure ($P/P_0 < 0.1$) over the PDC(n) samples of n = 0.35, 0.7 and 1. Correspondingly, a H_2-type hysteresis loop emerges and becomes clear at high IL contents. Table 1 lists the textural properties of these PDC(n) samples. With the low IL proportion, PDC(0.1) and PDC(0.17) synthesized in ethanol exhibit the low surface areas

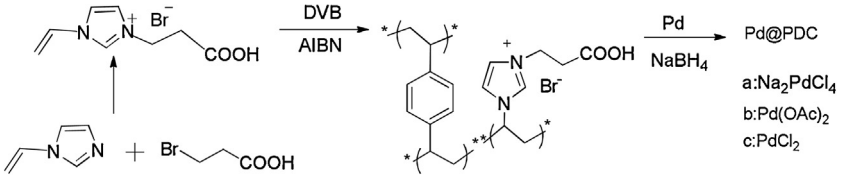

Scheme 1. Synthesis of Pd NPs loaded on poly(ionic liquid)s.

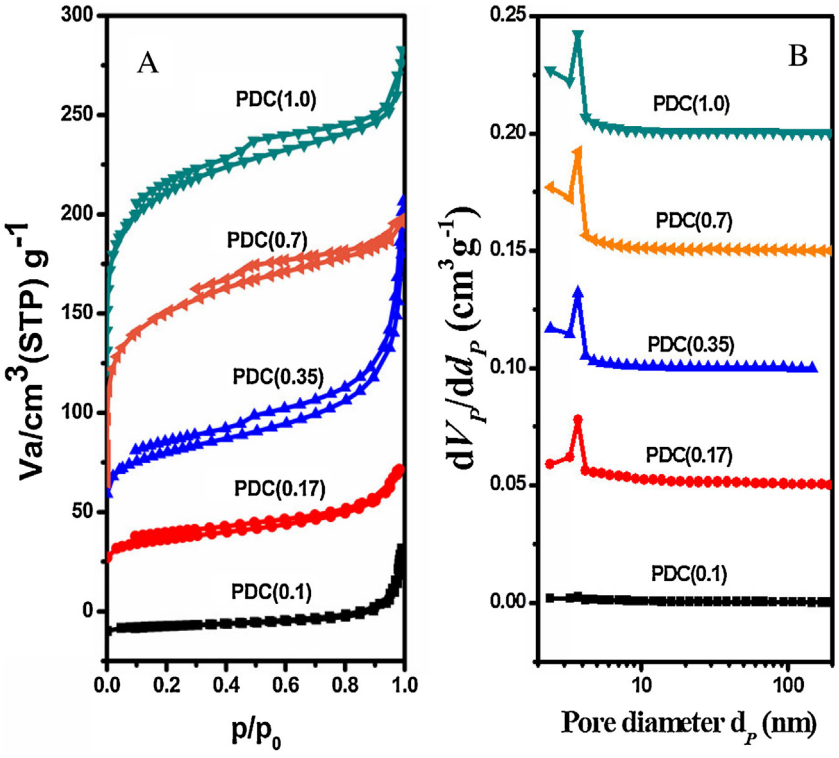

Fig. 1. (A) N_2 sorption isotherms and (B) pore size distribution curves of PDC(n) with different ionic liquid content.

of 10 and 39 $m^2 g^{-1}$. Enhancing the IL proportion and varying the solvent to the mixture of ethanol/water/ethyl acetate (5/5/25, v/v/v) results in the higher surface area (84 $m^2 g^{-1}$) and larger pore volume (0.201 $cm^3 g^{-1}$) over PDC(0.35) By using the same mixed solvent and increasing n to 0.7, PDC(0.7) reaches the high surface area (310 $m^2 g^{-1}$) and large pore volume (0.253 $cm^3 g^{-1}$). At such a condition, further increasing n to 1 brings about a decline of the surface area (174 $m^2 g^{-1}$) and pore volume (0.15 $cm^3 g^{-1}$) for PDC(1). The actual molar ratio of IL to DVB in the final copolymer product is calculated from the nitrogen content measured by elemental analysis for each PDC(n) sample (Table S1). It is seen that the actual IL content in PDC(n) is always lower than the IL amount in the starting synthetic solution, suggesting that DVB is more likely preserved in the copolymers. As for the IL molar content, Table 1 shows that PDC(0.1) and PDC(0.17) have a low level of 0.75 mmol g^{-1}. With increasing IL proportion in the synthetic system, IL content continuously increases and reaches the maximum value of 2.27 mmol g^{-1} for PDC(1). Therefore, above analyses indicate that by systematically varying the synthetic conditions, we can obtain an ionic copolymer PDC(0.7) that possesses a large surface area with relatively high IL content.

Scanning electron microscopy (SEM) images indicate that PDC(n) series are aggregations of micrometer-leveled particles (Fig. 2A, B and S5), similar to the homopolymer PDVB (Fig. 2I). After loaded with Pd NPs, the obtained Pd@PDC(0.7) sample also exhibits the morphology of particle aggregations but with certain fusion of the primary particles (Fig. 2H). Further, it has the surface area of about 40 $m^2 g^{-1}$ and pore volume of 0.0662 $cm^3 g^{-1}$ (Fig. S6). It is notable that its mother sample Pd(II)@PDC(0.7) (i.e., after ion-exchanging and before reduction) has the large surface area of 288 $m^2 g^{-1}$ and pore volume of 0.2048 $cm^3 g^{-1}$, suggesting well preserved porosity during the mere ion-exchanging process. Therefore, the decline of the surface area for Pd@PDC(0.7) sample can be attributed to blocking of micropores by therein created Pd NPs in the $NaBH_4$ reduction, as well as the most possible partial pore collapse induced by the explosively formed H_2 gases. Nonetheless, the preserved certain meso- and macro-pores in Pd@PDC(0.7) are still capable to afford enough mass transfer for heterogeneous catalysis because of the soft nature of the polymeric skeleton [41]. Inductively coupled plasma spectroscopy (ICP) analyses show that Pd weigh percentage in Pd@PDC(0.7) is 0.92 wt%, and a higher IL content favors the higher Pd content for these PDC(n) samples (Table 2, Entries 1–5). This observation implies that the IL unit in polymeric framework would have acted as an ion-exchanging site to uniformly anchor Pd(II) species, which is crucial for achieving a narrow dispersion of the finally formed Pd NPs after reduction. The transmission electron microscope (TEM) image of Pd@PDC(0.7) reveals the narrow distribution of Pd NPs over this ionic copolymer support (Fig. 2C). The average size of these Pd NPs is ca. 2.46 nm, at a

Table 2
Catalytic results of benzyl alcohol oxidation over Pd@MPIL.[a]

Entry	Catalyst	Pd Source	Pd wt%[b]	Conv. (%)[c]	Sel. (%)[d]	TON[e]
1	Pd@PDC(0.1)	Na_2PdCl_4	0.58	87	99	758
2	Pd@PDC(0.17)	Na_2PdCl_4	0.78	83	99	591
3	Pd@PDC(0.35)	Na_2PdCl_4	0.80	90	99	596
4	Pd@PDC(0.7)	Na_2PdCl_4	0.92/0.87[f]	96	99	553
5	Pd@PDC(1.00)	Na_2PdCl_4	1.62	86	99	281
6	Pd $(OAc)_2$@PDC(0.7)	$Pd(OAc)_2$	1.19	92	99	409
7	$PdCl_2$@ PDC(0.7)	$PdCl_2$	0.89	77	99	547
8	Pd@PDVB	Na_2PdCl_4	0.60	26	99	230
9	Pd@PIL-NH_2	Na_2PdCl_4	0.68	72	99	561
10	Pd@PIL-C_4H_9	Na_2PdCl_4	1.23	84	99	362
11	Pd@PIL-CN	Na_2PdCl_4	0.96	86	99	474

[a] Reaction conditions: 1 mmol benzyl alcohol, 1 mL water, 90 °C, 5 h, 0.02 g catalyst, 1 mmol K_2CO_3, O_2 balloon.
[b] Pd loading on the polymer support measured by inductively coupled plasma.
[c] Conversion = mmol (benzyl alcohol) converted/mmol (initial benzyl alcohol) × 100%.
[d] Selectivity of benzaldehyde = mmol (benzaldehyde)/mmol (benzyl alcohol converted) × 100%.
[e] TON = mol of product/moles of Pd content.
[f] For the recovered Pd@PDC(0.7) catalyst after the fifth recycling run.

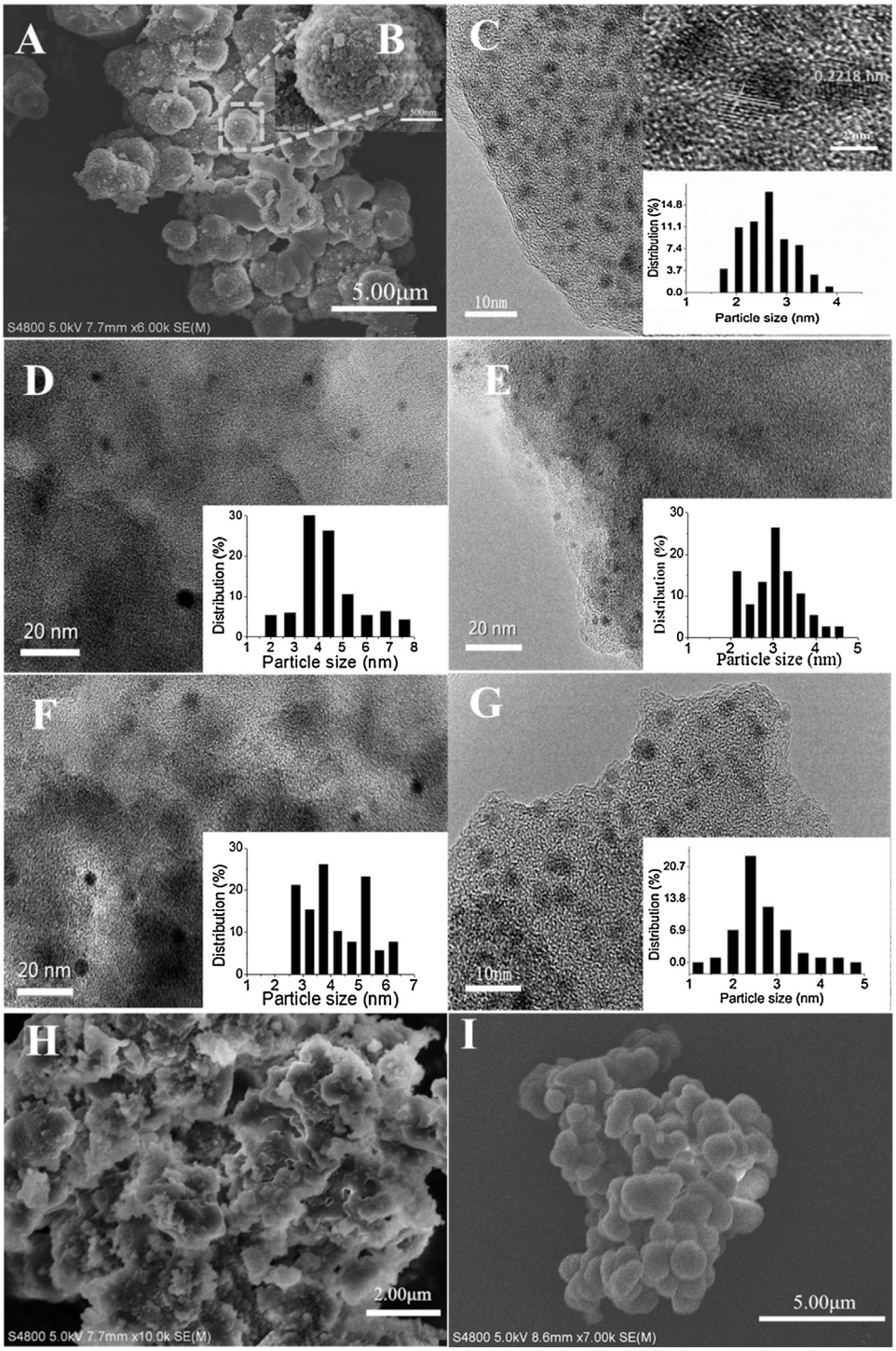

Fig. 2. SEM images of (A) and (B) PDC(0.7); H) Pd@PDC(0.7); (I) PDVB. TEM images of (C) Pd@PDC(0.7); (D) Pd@PIL-C_4H_9; (E) Pd@PIL-CN; (F) Pd@PIL-NH_2; (G) recovered Pd@PDC(0.7).

fine size level compared to those immobilized on general supports [5,42,43]. A clear regular lattice can be observed and the lattice distance is about 0.22 nm, index of Pd (111) as the most exposed crystal face, which is known active for benzyl alcohol reaction [44–46].

Figs. 3 A and S7 illustrate the FT-IR spectra of PDC(0.7), Pd(II)@PDC(0.7), Pd@PDC(0.7) and other functional MPILs. PDC(0.7) exhibits several characteristic peaks for the polymeric framework. The peaks at 3051 cm^{-1} and 3132 cm^{-1} are resulted from C—H stretching vibrations in the benzene ring, and those at 1158, 1577 and 1448 cm^{-1} show the existence of the imidazole ring [47]. Moreover, the bands at 2922 and 2847 cm^{-1} are ascribed to C—H stretching vibrations for —CH_2–, while the 1720 cm^{-1} band for C=O stretching vibration means the existing of carboxyl group in PDC(0.7) [48]. After Pd(II) loading through ion-exchanging with Na_2PdCl_4, the peak at 1720 cm^{-1} weakens while the intensity of the peak at 1580 cm^{-1} enhances. This implies the interaction of —COOH group with Na^+, and the thus formed —COO– species shows clearly the featured band at around 1580 cm^{-1}. After reduction with $NaBH_4$, the obtained Pd@PDC(0.7) sample exhibits much weak peak

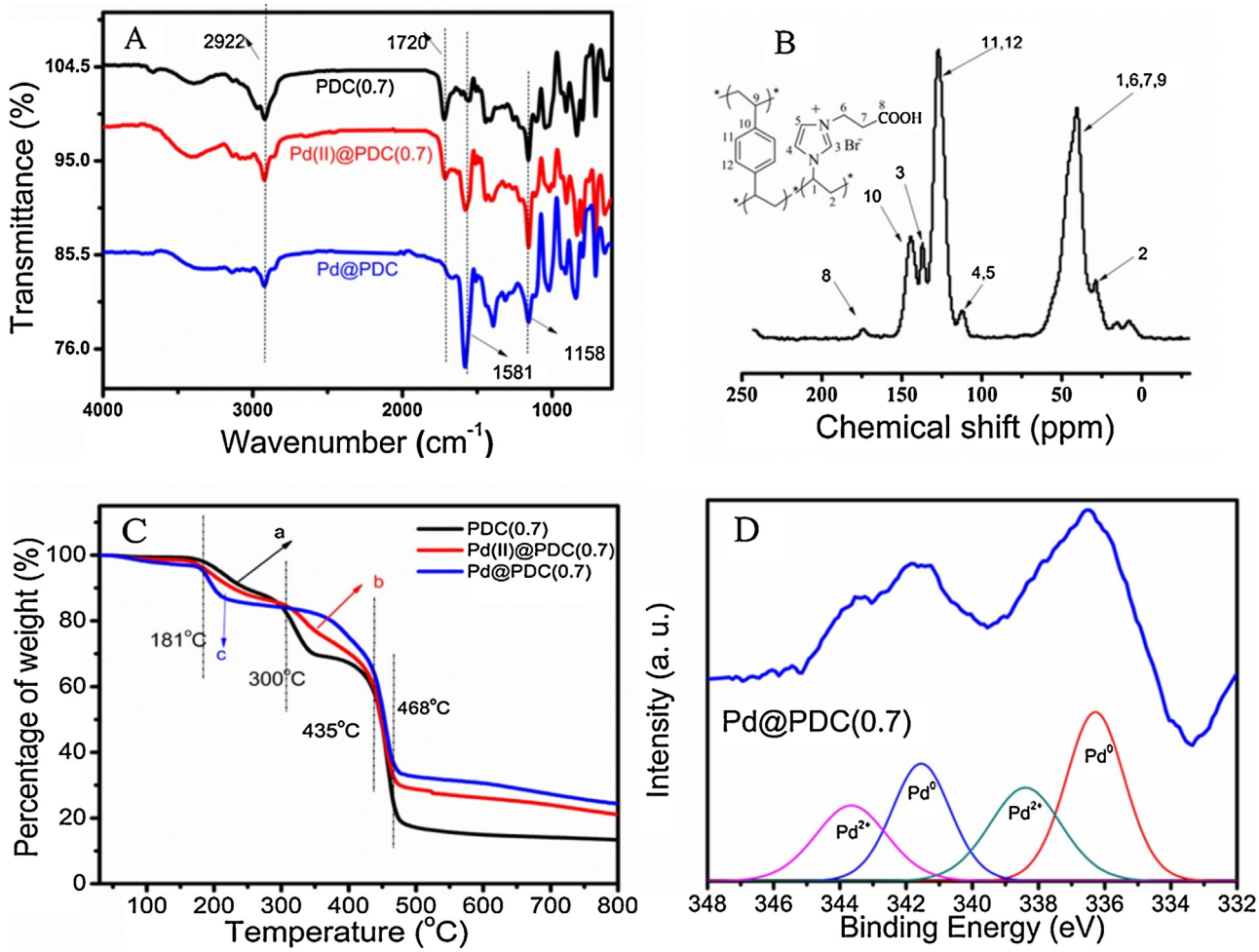

Fig. 3. (A) FT-IR spectra of PDC(0.7), Pd(II)@PDC(0.7) and Pd@PDC(0.7); (B) ^{13}C MAS NMR spectra of PDC(0.7); (C) TG curves of (a) PDC(0.7), (b) Pd(II)@PDC(0.7) and (c) Pd@PDC(0.7); (D) XPS of Pd@PDC(0.7).

at 1720 cm^{-1} and further enhanced adsorption band at 1580 cm^{-1}, due to the additional consumption of —COOH to form —COO—.

Fig. 3B depicts the solid state ^{13}C NMR spectra of PDC(0.7). The chemical shift peak at around 32 ppm corresponds to the methylene unit that is connected with other carbon atoms in the alkyl chain. The broad overlapping peak at 42 ppm is attributed to the four carbon atoms attached to imidazole ring and benzene ring, and the strong one at 128 ppm is ascribed to the C11 and C12 atoms while 145 ppm is attributed to C10 atom of the benzene ring. For the imidazole ring, the peak at 111 ppm is index of C4 and C5 atoms, and C3 atom is reflected by the single one at 136 ppm [40]. These observations confirm the existence of imidazolium cation unit in the polymeric backbone, and also reflect the copolymerization of DVB and IL precursor, as shown in Scheme 1 for the chemical structure. More insightfully, a very weak signal at 174 ppm is detected, implying the formation of carboxyl carbon atom (C8) in the polymer structure [49].

TG curves for PDC(0.7), Pd(II)@PDC(0.7) and Pd@PDC(0.7) (Fig. 3C) show the weight loss in ranges of 30–181, 181–300 and 435–468 °C, respectively. The initial weight loss at low temperatures is ascribed to the release of physical adsorbed water due to the hydrophilic nature of IL units in the ionic copolymeric framework. By contrast, PDVB exhibits rare weight loss at 30–300 °C due to its hydrophobic skeleton (Fig. S8A). Decomposition of functional imidazolium units begins at 181 °C for both PDC(0.7) and Pd@PDC(0.7) [50]. The successive degradation of polymeric networks starts at 300–435 °C for PDC(0.7), Pd(II)@PDC(0.7) and Pd@PDC(0.7). Above all, Pd@PDC(0.7) exhibits the lowest decomposition rate, reflecting an enhanced thermal stability after loaded with Pd NPs. Complete weight loss ends at about 468 °C for three samples, similar to PDVB. XRD patterns recorded for PDC(0.7) and Pd@PDC(0.7) show only very broad peaks at around 20.0 and 22.5° respectively (Fig. S8B), reflecting an amorphous structure. No Pd characteristic peak appears, confirming the high dispersion of these ultrafine Pd NPs and excluding their possible agglomeration.

Further, metallic nature and oxidation state of Pd NPs in Pd@PDC(0.7) is investigated by X-ray photoelectron spectroscopy (XPS). Fig. S9A shows the survey scan spectrum of Pd@PDC(0.7). The peaks with binding energies of ca. 283.5, 530 and 340 eV are attributed to C 1s, O 1s and Pd 3d, respectively, confirming the presence of C, O and Pd elements in the catalyst. Fig. 3D shows the XPS signals in the binding energy region of 332–348 eV, which is fitted with multiple peaks. Two sets of doublet peaks corresponding to Pd $3d_{5/2}$ and Pd $3d_{3/2}$ can be observed on Pd 3d spectrum [51]. The relatively lower binding energy set of spin-orbit doublet at 336.2 ($3d_{5/2}$) and 341.5 eV ($3d_{3/2}$) is attributed to Pd(0) species, and the other set of doublet at 338.2 ($3d_{5/2}$) and 343.7 eV ($3d_{3/2}$) is to Pd(II) species. Especially, the Pd 3d core level is deconvoluted into two spin-orbit split components with binding energies of 336.2 and 338.2 eV [52]. The component at 336.2 eV is assigned to Pd(0), slightly higher than the one for clean Pd metal (~334.6 eV) [53]. The component at 338.2 eV is identified as Pd(II) species because of above shift in the binding energy scaled by about 1.6 eV. Quantitative calculation from the peak area in Fig. 3D indicates that the major part of the

Pd NPs is Pd(0); also as predicted, partial of them is in the state of Pd(II) because the surface of Pd NPs is much easily reoxidized when exposed in air though stored in a desiccator. For detailed comparison of the C 1s and O 1s XPS data between Pd@PDC(0.7) and its support PDC(0.7) (Fig. S9B and C), there is rare difference in their C 1s curves; however the O 1s peak of Pd@PDC(0.7) shows a remarkable downshift toward lower binding energy by ca. 1 eV compared with PDC(0.7). This implies that the carbon-backbone of the polymer is unaltered upon the loading of Pd NPs into PDC(0.7), but there should have occurred another binding pattern on O atoms other than the original group —COOH [54]. Accordingly, we suppose that the downshift of O 1s peak reflects the formation of coordination interaction of the —COO− ligand with the surface of Pd NPs, which is in good agreement with our observation of —COO− group from FT-IR spectra.

Overall, the above characterizations allow drawing that, through the anion-exchange of the support PDC(0.7) in aqueous solution of Na_2PdCl_4, the intermediate sample Pd(II)@PDC(0.7) is obtained; at this moment, the Pd species occur as the $PdCl_4^{2-}$ free ions, countering against the cationic sites on the ionic liquid units of the copolymer backbone. Pd(II)@PDC(0.7) shows a large surface area because the enable the $PdCl_4^{2-}$ free ions cannot effectively block the meosporous channels. Upon the further chemical reduction by $NaBH_4$, the final catalyst Pd@PDC(0.7) is resulted; in this case the Pd species appear as the Pd(0) NPs with partial of them reoxidized into Pd(II) state due to exposure in air. The approved coordination affinity of the functional carbonyls tethered on the copolymer backbone with the surface Pd species contributes significantly to the narrow size distribution of Pd NPs. The surface area of Pd@PDC(0.7) is remarkably lowered down; however, still a considerable surface area of 40 $m^2 g^{-1}$ is remained with existence of meso- and macropores, which would be important for its performance as a heterogeneous catalyst.

3.2. Catalytic tests in the oxidation of benzyl alcohol

Catalytic performances of the Pd@PDC(n) series are assessed in the oxidation of benzyl alcohol to benzaldehyde with oxygen balloon by using water as the solvent at the low temperature of 90 °C. Catalysis assessment starts with the optimization of Pd@PDC(0.7) sample by varying the reaction time and temperature (Fig. S10). At 90 °C, the conversion continuously increases with reaction time, and reaches a high value of 94% at 4 h. Further increasing the reaction time to 5 h gives a slightly higher conversion of 96%. No by-product is detected, index of a high selectivity of >99%. Fixing the reaction time at 5 h, a higher temperature favors higher conversion until 90 °C. Up to 100 °C, the conversion no longer goes higher but accompanies with a slight decrease in selectivity. The result suggests that 90 °C and 5 h are optimal conditions for this reaction. Under the similar conditions, catalytic activities of Pd NPs catalysts supported on various other polymers are parallel assessed, as listed in Table 2. Pd@PDC(0.1) gives a lower conversion of 83% than Pd@PDC(0.7), attributable to the relatively low Pd content of the former. For Pd@PDC(n) series, as the IL content increases, more Pd NPs are loaded on the supports; therefore, the conversion continuously increases up to n = 0.7. Nonetheless, Pd@PDC(1) presents the inferior conversion of 86% in spite of high IL content and Pd loading amount. This seemingly unusual result associates with the suppose that the high density of the IL unit can anchor highly abundant Pd(II) via ion-exchange, but will cause the aggregation of Pd NPs during the reduction process. Such phenomena indicate that both composition and pore structure should be suitable to benefit the formation of highly active Pd NPs on MPIL support. Thus PDC(0.7) possessing a large surface area and moderate IL content acts as a suitable support for Pd NPs with high catalytic efficiency.

For better understanding effect of ionic unit of the polymer support, Pd NPs supported on homopolymer PDVB is tested. PDVB is a neutral backbone polymer with a large surface area of 259 $m^2 g^{-1}$ and pore volume of 0.195 $cm^3 g^{-1}$. Owing to the existence of partial micropores, as demonstrated by the uptake below $P/P_0 < 0.1$ in nitrogen sorption isotherm (Fig. S11A), Pd(II) precursors can be adsorbed on PDVB and successively reduced to Pd NPs. Catalysis test shows that Pd@PDVB gives only very low conversion of 26%, though it contains 0.6 wt% Pd that is similar to Pd@PDC(0.1). The reason can be attributed to lack of ionic sites in neutral skeleton of PDVB that is unable to provide sufficient affinity to disperse Pd(II) and the corresponding Pd NPs. This phenomenon confirms the advantage of MPILs for preparing highly and even uniformly dispersed Pd NPs through an ion-exchanging and reduction route.

For further comparison, various MPILs tethered with other groups of cyano, amino and alkyl are prepared and used for Pd NPs supports. Synthesis conditions including the initial IL content are same as PDC(0.7). Nitrogen sorption results reveal that they are all typical mesoporous materials with the surface area of about 100 $m^2 g^{-1}$. Elemental analyses give the order of IL contents for these polymers (Table 1): PIL-C_4H_9 (2.16 mmol g^{-1}) > PIL-CN (0.96 mmol g^{-1}) > PIL-NH_2 (0.5 mmol g^{-1}), well corresponding to that of Pd loadings (Table 2): Pd@PIL-C_4H_9 (1.23 wt%) > Pd@PIL-CN (0.96 wt%) > Pd@PIL-NH_2 (0.68 wt%). TEM images (Fig. 2D–F) show that Pd@PIL-NH_2 exhibits larger average size of Pd NPs (ca. 4.1 nm), though with the lowest Pd content, than that for Pd@PIL-C_4H_9 (3.8 nm) and Pd@PIL-CN (3.2 nm). Moreover, compared with the lead catalyst Pd@PDC(0.7) with the carbonyl functional group, the three catalysts show not only larger average size of Pd NPs but broader size distribution. All the three controls are assessed in the oxidation of benzyl alcohol to benzaldehyde. Pd@PIL-NH_2 gives a conversion of 72%, inferior to that of Pd@PIL-C_4H_9 (84%) and Pd@PIL-CN (86%), closely relative to its low content and large size of Pd NPs. Interestingly, the alkyl group in PIL-C_4H_9 is incapable to coordinate with Pd(II) species or provide additional stabilization effect to immobilize Pd NPs, yet, much higher yield of 84% than the one over PDVB (26%) is observed by Pd@PIL-C_4H_9. The result implies that the Pd(II) species are immobilized mainly through the ion-exchanging process and the ionic sites in the ionic copolymeric skeleton significantly contribute to the high efficiency of Pd NPs. Further, Pd@PIL-C_4H_9 and Pd@PIL-CN demonstrate much inferior activity to Pd@PDC(0.7), mostly due to their larger average size and broader size distribution of Pd NPs. Especially, PDC(0.35) and PIL-CN have same IL content and surface area, but Pd NPs supported on the former exhibits better activity than that on the latter even with a lower Pd content. These phenomena show that IL monomer with the carbonyl group acts as an important component in the copolymeric skeleton to achieve highly efficient Pd NPs.pt

Besides, two other palladium precursors, $Pd(OAc)_2$ and $PdCl_2$, are used for preparing Pd NPs on PDC(0.7) with the similar loading process as Pd@PDC(0.7). The corresponding catalysts are denoted as Pd@PDC(0.7)-$Pd(OAc)_2$ and Pd@PDC(0.7)-$PdCl_2$. They contain 1.19 and 0.89 wt% Pd, and give the conversions of 92% and 77%, respectively. The lower conversion than that over Pd@PDC(0.7) is due to the varied bonding mode of Pd(II) to the supports, which is derived from different Pd sources. When Na_2PdCl_4 is used, $PdCl_4^{2-}$ anions can be subjected to the desirable ion-exchange with Br− in the mesopores of ionic polymers, and the Pd(II) can be firmly fixed to the support with strong ionic bond [55]. Such stable host-guest interaction not only helps the highly dispersion of Pd(II) species, but also favors to stabilize and inhibit the agglomeration of Pd(0) NPs during the reduction and successive catalytic process [29]. By contrast, $Pd(OAc)_2$ and $PdCl_2$ can only interact with the support through the weak coordination mode, thus are disadvantageous for the formation of highly dispersed Pd NPs. Pd(II) has a strong

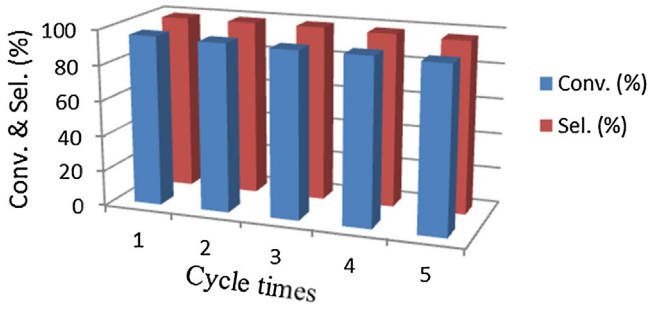

Fig. 4. Recycle ability of catalyst Pd@PDC(0.7) for oxidation of benzyl alcohol.

interaction with Cl−, weakening the interaction with the support, thus less Pd NPs can be loaded with inferior activity by using $PdCl_2$.

At the finish of a reaction, the solid catalyst Pd@PDC(0.7) can be conveniently separated by filtration. With the further washing with ethanol for three times and vacuum drying at 80 °C for 6 h, the recovered catalyst is recharged into the next run for recycling test. The catalytic reusability of Pd@PDC(0.7) investigated in a five-run recycling test is shown in Fig. 4. No apparent decline of conversion and selectivity happens, reflecting stable activity during the reuse process. The well reusability can be assigned to the preservation of polymeric framework and stable Pd NPs during the reaction. After the fifth run, the TEM image indicates that still uniform and narrow dispersed Pd NPs can be preserved, and the average particle size is about 2.60 nm, very close to the value over the fresh catalyst (2.46 nm). (Fig. 2F) Considering the experimental error, it can be regarded that rare variation happens on the average particle size of these Pd NPs. On the other hand, ICP analysis results for the Pd loadings of the fresh catalyst (0.92%) and the recovered one (0.87%) (Table 2) reveal that 94% Pd NPs are preserved in the five-time reused catalyst, further confirming the stable Pd NPs and accounting for the well remained activity during the catalyst recycling.

The activity and stability of supported NPs are crucial for their practical applications. Various noble metals (Pd, Au or Pd/Au) NPs have been prepared by using different supports for aerobic oxidation of benzyl alcohol; some of them even exhibited efficiency at very mild conditions such as room temperature and ambient pressure. Nonetheless, most of them still suffered from the decline of activity after several times reuse, as shown in Table S2. Compared to previous works, Pd@PDC(0.7) gives a high and stable efficiency with a low Pd dosage (0.17% to substrate) for the low-temperature aerobic oxidation of benzyl alcohol to benzaldehyde (details of comparison are described in Table S2). Besides, high efficiency is obtained by using water as the sole solvent rather than harmful organic solvent, thus the catalysis features as a green and sustainable process. Further, we also investigate the performance of Pd@PDC(0.7) in solvent-free aerobic oxidation of benzyl alcohol to benzaldehyde at elevated temperature. In a roughly test without optimization, Pd@PDC(0.7) offers a yield of 17% with high selectivity of >99% (reaction condition: 50 mmol benzyl alcohol, 160 °C, 1 h, catalyst 0.01 g, 1 mmol K_2CO_3, O_2 balloon). With elevated reaction time to 5 h, the yield arises up to 33% with selectivity of >95%. The turnover number (TON = mol of product/moles of Pd) is 10474 and 20331 at 1 and 5 h, respectively. Such activity is also better or at least comparable to the most efficient supported Pd NPs for solvent-free aerobic benzyl alcohol oxidation to benzaldehyde (Table S2). The comparative analysis further confirms the high catalytic efficiency of Pd@PDC(0.7).

3.3. Insight into the catalytic behavior

As demonstrated above, Pd NPs supported on ionic copolymer tethered with −COOH group show very efficient and stable catalytic activity in the oxidation of benzyl alcohol to benzaldehyde with O_2 by using water as the sole solvent. Because the substrate benzyl alcohol is only sparingly soluble in water, the catalytic process involves four phases: gas (O_2), solid (catalyst), oil (organic substrate) and water. Thus, the reaction is actually a

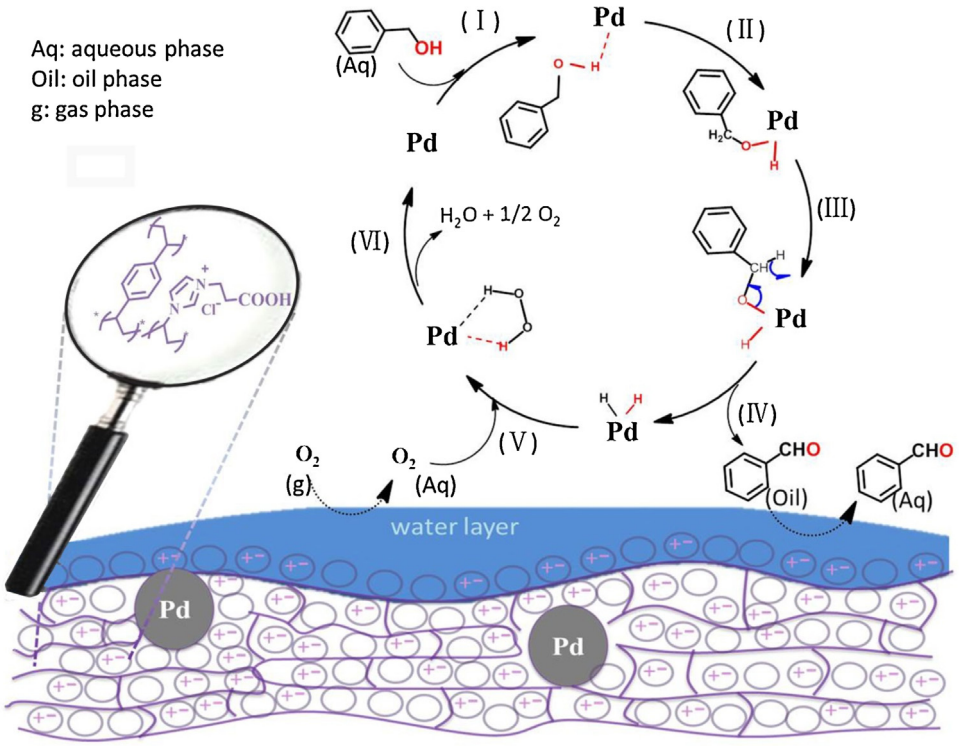

Scheme 2. Proposed catalytic cycle for oxidation of benzyl alcohol.

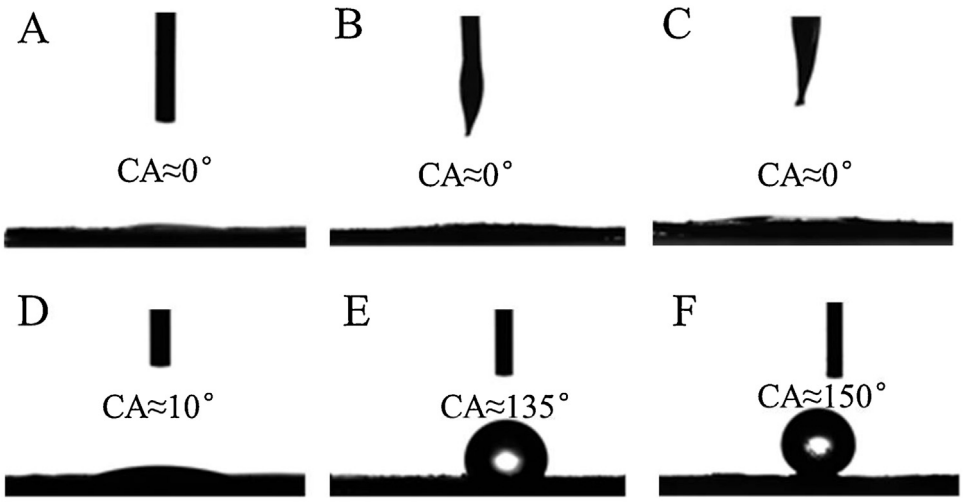

Fig. 5. Contact angles of (A) water droplet, (B) Benzyl alcohol droplet, (C) benzaldehyde droplet on the surface of Pd@PDC(0.7) and water droplet of (D) Pd@PDC(0.35), (E) Pd@PDC(0.17) and (F) PDVB.

gas-liquid-liquid-solid quadruple-phase system. Scheme 2 illustrates the proposed reaction route. Ionic sites in the organic framework, similar to the behavior of ILs [56–58], possess strong affinity to H_2O. In the aqueous phase reaction, water is chemically adsorbed on these hydrophilic ionic sites to generate a layer of water with abundant dangling −OH groups on the surface, according to previous studies on IL-water interaction [59,60]. Consequently, the surface −OH groups at oil-water interface act as H-bond donor to promote the interaction between the substrate (benzyl alcohol) and water, and accelerates the diffusion of benzyl alcohol molecules into water layer on the catalyst surface. Diffused benzyl alcohol molecules are thus easily accessible to the active sites, Pd(0) species that just locates on these ionic sites. Through above interaction of benzyl alcohol with the coordinately unsaturated Pd at the nanoparticle edge, the intermediate Pd-alcoholate forms, which then undergo a β-hydride elimination to give the target product benzaldehyde. The formed benzaldehyde is well water-soluble and can be timely expelled from a water layer, through which the reaction equilibrium forward shifting is accelerated and the high selectivity is obtained by avoiding further oxidation. At the same time, Pd-hydride species is created that is then oxidized by the O_2 dissolved in the water layer, which ultimately regenerates the original Pd(0) state with releasing of H_2O and O_2.

In this reaction route, water as the solvent is not only cheap, green and nontoxic, but also increases the concentration of dissolved O_2 compared to common organic solvents, thus benefits the regeneration of Pd(0) species. Ionic sites in hydrophobic DVB framework construct a suitable hydrophilic/hydropholic surface that allows dual wettability for water and benzyl alcohol. This is confirmed by the contact angle analyses of water, benzyl alcohol and benzaldehyde on the surface of Pd@PDC(0.7) (Fig. 5A, 5B and 5C), in which all the three probe molecules can rapidly and almost completely spread on its surface, thus providing accessible reaction microenvironment for this multiphase reaction. The more ionic sites, the stronger hydrophilic behavior on the support surface for PDC(0.35) and PDC(0.17) (Fig. 5D, 5E), and the water contact angle reaches up to 150° (Fig. 5F) for neat PDVB. Because of the amphiphilic nature, it is not surprising that the catalyst Pd@PDC(0.7) can also give good result for the oxidation of benzyl alcohol into benzaldehyde when toluene is used as the organic solvent (conversion 99% and selectivity 95%, 4 h) instead of water under the otherwise similar conditions. Besides the hydrophilic/hydropholic property, the remained meso- and macropores in Pd@PDC(0.7) facilitate the fast mass transfer that is crucial in heterogeneous catalysis. The ionic liquid unit of in this copolymer matrix plays crucial roles in the following items. (1) Abundant ionic sites on the large-surface-area mesopore walls of the copolymer material enable the high dispersion of $PdCl_4^{2-}$ free ions through anion-exchanging. (2) The in situ functional groups like −COOH tethered on ionic liquid closely associate with the narrow size distribution of the resultant Pd NPs upon chemical reduction by providing strong coordination affinity. (3) The hydrophilicity of ionic liquid monomer due to its strong electrostatic field for polarizing water and the hydrophobicity of another monomer DVB bring about the special well amphiphilicity of the obtained copolymer, which accounts for the superior activity for water-mediated oxidation of benzyl alcohol. (4) During the reaction, the ionic liquid unit in the copolymer backbone also contributes significantly to the stabilization the Pd NPs by inhibiting their agglomeration. In a word, the tunable ionic copolymeric framework is responsible for the preparation of fine Pd NPs and favorable to the microenvironment for the multi-phase reaction. It is also expected that noble metal nanoparticles supported on MPILs would be able to demonstrate further potential applications in other reactions by controlling their compositions and structures.

4. Conclusion

Narrow distributed and highly dispersed palladium (Pd) nanoparticles (NPs) with the size of 2–3 nm are fabricated on the carboxyl functional MPILs through controlling the copolymerization of task-specific IL monomer and DVB. The ionic polymeric skeleton with −COOH group provides sufficient affinity toward high dispersion of Pd(II) precursors during the ion-exchanging process, and also serves as the stabilizer for the formation of Pd(0) NPs during the reduction and catalysis processes. The obtained lead catalyst Pd@PDC(0.7) exhibited high efficiency and well reusability in the selective oxidation of benzyl alcohol to benzaldehyde under mild conditions of oxygen balloon at 90 °C by using water as the sole solvent. The present work provides an efficient heterogeneous recyclable catalyst for benzyl alcohol oxidation and outlines that stable functional metal NPs can be reasonably fabricated through adjusting the ionic polymer framework.

Acknowledgements

The authors thank greatly the National Natural Science Foundation of China (Nos. 21136005 and 21303084 and 21476109), Jiangsu Provincial Science Foundation for Youths (No. BK20130921), Specialized Research Fund for the Doctoral Program of Higher Education (No. 20133221120002).

Appendix A. Supplementary data

Supplementary data associated with this article can be found, in the online version, at http://dx.doi.org/10.1016/j.apcatb.2016.02.067.

References

[1] G. Liu, M.Q. Hou, J.Y. Song, T. Jiang, H.L. Fan, Z.F. Zhang, B.X. Han, Green Chem. 12 (2010) 65–69.
[2] M.L. Zou, M.L. Du, M. Zhang, T.T. Yang, H. Zhu, P. Wang, S.Y. Bao, Mater. Res. Bull. 61 (2015) 375–382.
[3] P. Weerachawanasaka, G.J. Hutchingsb, J.K. Edwardsb, S.A. Kondratb, P.J. Miedziakb, P. Praserthama, J. Panpranota, Catal. Today 250 (2015) 218–225.
[4] Q.H. Yang, Y.Z. Chen, Z.Y. Wang, Q. Xu, H.L. Jiang, Chem. Commun. 51 (2015) 10419–10422.
[5] T. Yuan, H.F. Gong, K. Kailasam, Y.X. Zhao, A. Thomas, J.J. Zhu, J. Catal. 326 (2015) 38–42.
[6] H.L. Parker, J.R. Dodson, V.L. Budarin, J.H. Clarka, A.J. Hunt, Green Chem. 17 (2015) 2200–2207.
[7] X.Y. Wan, C.M. Zhou, J.S. Chen, W.P. Deng, Q.H. Zhang, Y.H. Yang, Y. Wang, ACS Catal. 4 (2014) 2175–2185.
[8] Z.H. Zhang, J.D. Zhen, B. Liu, K.L. Lv, K.J. Deng, Green Chem. 17 (2015) 1308–1317.
[9] K. Layek, H. Maheswaran, R. Arundhathi, M.L. Kantam, S.K. Bhargava, Adv. Synth. Catal. 353 (2011) 606–616.
[10] H.L. Wu, Q.H. Zhang, Y. Wang, Adv. Synth. Catal. 347 (2005) 1356–1360.
[11] Y. Li, X. Xu, P.F. Zhang, Y.T. Gong, H.R. Li, Y. Wang, RSC Adv. 3 (2013) 10973–10982.
[12] G.L. Zhuang, J.Q. Bai, L. Tan, H.L. Huang, Y.F. Gao, X. Zhong, C.L. Zhong, J.G. Wang, RSC Adv. 5 (2015) 32714–32719.
[13] S.B. Kalidindi, H. Oh, M. Hirscher, D. Esken, C. Wiktor, S. Turner, G.V. Tendeloo, R.A. Fischer, Chem. Eur. J. 18 (2012) 10848–10856.
[14] S.I. Yamamoto, H. Kinoshita, H. Hashimotob, Y. Nishina, Nanoscale 6 (2014) 6501–6505.
[15] Y.P. Yu, T.J. Hu, X.R. Chen, K.L. Xu, J.L. Zhang, J. Huang, Chem. Commun. 47 (2011) 3592–3594.
[16] Y. Chen, Z. Guo, T. Chen, Y. Yang, J. Catal. 275 (2010) 11–24.
[17] J. Li, X.Y. Shi, Y.Y. Bi, J.F. Wei, Z.G. Chen, ACS Catal. 1 (2011) 657–664.
[18] J. Artz, S. Mallmann, R. Palkovits, ChemSusChem 84 (2015) 672–679.
[19] J.C. Li, P.H. Zeng, L. Zhao, S.Y. Ren, Q.X. Guo, H.J. Zhao, J. Catal. 329 (2015) 441–448.
[20] F. Anaya, L. Zhang, Q.H. Tan, D.E. Resasco, J. Catal. 328 (2015) 173–185.
[21] J.C. Li, P.H. Zeng, L. Zhao, S.Y. Ren, Q.X. Guo, H.J. Zhao, B.J. Wang, H.H. Liu, X.M. Pang, X.H. Gao, B.J. Shen, J. Catal. 329 (2015) 441–448.
[22] G.R. Reddy, S.B.K. Chennakesavulu, RSC Adv. 5 (2015) 81013–81023.
[23] S.G. Zhang, K.R. Dokkoa, M. Watanabe, Chem. Sci. 6 (2015) 3684–3691.
[24] H.L. Han, T. Jiang, T.B. Wu, D.X. Yang, B.X. Han, ChemCatChem 7 (2015) 3526–3532.
[25] Y. Leng, J. Wang, D.R. Zhu, M.J. Zhang, P.P. Zhao, Z.Y. Long, J. Huang, Green Chem. 13 (2011) 1636.
[26] C.J. Gao, G.J. Chen, X.C. Wang, J. Li, Y. Zhou, J. Wang, Chem. Commun. 51 (2015) 4969–4972.
[27] X.C. Wang, Y. Zhou, Z.J. Guo, G.J. Chen, J. Li, Y.M. Shi, Y.Q. Liu, J. Wang, Chem. Sci. 6 (2015) 6916–6924.
[28] G.J. Chen, Y. Zhou, X.C. Wang, J. Li, S. Xue, Y.Q. Liu, Q. Wang, J. Wang, Sci. Rep. 5 (2015) 11236.
[29] P.F. Zhang, Z.A. Qiao, X.G. Jiang, G.M. Veith, S. Dai, Nano Lett. 15 (2015) 823–828.
[30] S. Bahadorikhalili, L. Mamani, H. Mahdavi, A. Shafiee, RSC Adv. 5 (2015) 71297–71305.
[31] D. Stuart, F. Miller, B. Holger, E. Friedrich, W. Holzapfel, D. Venkata, ChemCatChem 7 (2015) 2628–2636.
[32] C.C. Cassol, A.P. Umpierre, G. Machado, S.I. Wolke, J. Dupont, J. Am. Chem. Soc. 127 (2005) 3298–3299.
[33] D. Zhang, C.S. Zhou, R.H. Wang, Catal. Commun. 22 (2012) 83–88.
[34] J. Zhang, S.F. Lu, Y. Xiang, P.K. Shen, J. Liu, S.P. Jiang, ChemSusChem 8 (2015) 2956–2966.
[35] Y. Yan, Y.T. Chen, X.L. Jia, Y.H. Yang, Appl. Catal. B 156 (2014) 385–397.
[36] Y.T. Chen, H.J. Zheng, Z. Guo, C.M. Zhou, C. Wang, A. Borgna, Y.H. Yang, J. Catal. 283 (2011) 34–44.
[37] Y. Zhou, Z.H. Xiang, D.P. Cao, C.J. Liu, Ind. Eng. Chem. Res. 53 (2014) 1359–1367.
[38] H.W. Wang, C.L. Wang, H. Yan, H. Yi, J.L. Lu, J. Catal. 324 (2015) 59–68.
[39] X.P. Feng, C.J. Gao, Z.J. Guo, Y. Zhou, J. Wang, RSC Adv. 4 (2014) 23389–23395.
[40] X.C. Wang, J. Li, G.J. Chen, Z.J. Guo, Y. Zhou, J. Wang, ChemCatChem 7 (2015) 993–1003.
[41] J. Du, X.Y. Lai, N.L. Yang, J. Zhai, D. Kisailus, F.B. Su, D. Wang, L. Jiang, ACS Nano 5 (2011) 590–596.
[42] B. Helms, J.L. Mynar, C.J. Hawker, J.M. Frechet, J. Am. Chem. Soc. 126 (2004) 15020–15021.
[43] Q.H. Yang, Y.Z. Chen, Z.Y. Wang, Q. Xu, H.L. Jiang, Chem. Commun. 51 (2015) 10419.
[44] D. Ferri, C. Mondelli, F. Krumeich, A. Baiker, J. Phys. Chem. B 110 (2006) 22982–22986.
[45] C. Mondelli, D. Ferri, J.D. Grunwaldt, F. Krumeich, S. Mangold, R. Psaro, A. Baiker, J. Catal. 252 (2007) 77–87.
[46] Y.T. Chen, H.P. Wang, C.J. Liu, Z.Y. Zeng, H. Zhang, C.M. Zhou, X.L. Jia, Y.H. Yang, J. Catal. 289 (2012) 105–117.
[47] A. Pourjavadi, S.H. Hosseini, Z.S. Emami, Chem. Eng. J. 232 (2013) 453–457.
[48] D.D. Xiao, D.Q. Zhang, B.H. Chen, D.H. Xie, Y.J. Xiang, X.Y. Li, W.S. Jin, Langmuir 31 (2015) 10649–10655.
[49] J.B. Xu, J.X. Yang, X.D. Ye, C.F. Ma, G.Z. Zhang, S. Pispas, J. Polym. Sci. Part A: Polym. Chem. 53 (2015) 846–853.
[50] P.P. Zhao, J. Wang, G.J. Chen, Y. Zhou, J. Huang, Catal. Sci. Technol. 3 (2013) 1394–1404.
[51] E.V. Johnston, O. Verho, M.D. Krks, M. Shakeri, C.W. Tai, P. Palmgren, K. Eriksson, S. Oscarsson, J.E. Bckvall, Chem. Eur. J. 18 (2012) 12202–12206.
[52] P.F. Siril, L. Ramos, P. Beaunier, P. Archirel, A. Etcheberry, H. Remita, Chem. Mater. 21 (2009) 5170–5175.
[53] V. Schenck, J. Weissenrieder, S. Helldn, B. kermark, M. Gcthelid, Appl. Surf. Sci. 212 (2003) 508–514.
[54] V.Z. Radkevich, T.L. Senko, K. Wilson, L.M. Grishenko, A.N. Zaderko, V.Y. Diyuk, Appl. Catal. A: Gen. 335 (2008) 241–251.
[55] Y. Chen, Z. Guo, T. Chen, Y. Yang, J. Catal. 275 (2010) 11–24.
[56] A. Wilke, J.Y. Yuan, M. Antonietti, J. Weber, ACS Macro Lett. 1 (2012) 1028–1031.
[57] Q. Zhao, P. Zhang, M. Antonietti, J. Yuan, J. Am. Chem. Soc. 134 (2012) 11852–11855.
[58] Q. Zhao, M. Yin, A.P. Zhang, S. Prescher, M. Antonietti, J. Yuan, J. Am. Chem. Soc. 135 (2013) 5549–5552.
[59] S.G. Zhang, K.R. Dokko, M. Watanabe, Chem. Sci. 6 (2015) 3684–3691.
[60] J. Zhu, P.C. Wang, M. Lu, Appl. Catal. A 477 (2014) 125–131.